

Article

Defect Detection in Grouting Sleeve Grouting Material by Piezoelectric Wave Method

Qiyun Qiao ^{1,*}, Xiuyu Wang ¹, Wenchao Liu ² and Hongchun Yang ²

¹ Urban Construction Department, Beijing University of Technology, Beijing 100020, China; wangxiuyu@emails.bjut.edu.cn

² CCCC Construction Group Co., Ltd., Beijing 100120, China; liuwenchao2@ccccltd.cn (W.L.)

* Correspondence: qiaoyun@bjut.edu.cn

Abstract: The construction defects in grouting sleeves can jeopardize the safety of precast reinforced concrete structures. Thus, efficient and accurate defect detection is critical in engineering construction. In this paper, a defect detection method based on piezoelectric wave theory was proposed. Two piezoelectric ceramics were arranged within the grouting sleeve. One piezoelectric ceramic was affixed on the top of the steel bar, while the other was embedded in the grouting material, serving as the driver and sensor, respectively. The compactness defects, air cavity defects, steel anchoring defects, and water–binder ratio defects were set in the grouting sleeves, and the trends in time domain signals and signal evaluation indicators based on the wavelet packet total energy value (WPTEV) of different specimens were investigated. Based on the WPTEV, the evaluation index (*EI*) was proposed. In addition, the effect of the grouting material’s age on the piezoelectric wave signal was verified. Furthermore, the influence of grouting material defects on signals was simulated in ABAQUS, and the time domain signals and wavelet packet energy of sensor signals for specimens with varying defect dimensions were evaluated. The results showed that: (1) The defects in the grouting materials reduced the stress waves propagated through the grouting materials, resulting in a decrease in attenuation and an increasing trend in the signal; (2) The peak-to-peak values of piezoelectric ceramic sensors and the WPTEV of the signal increased with the degree of defects, and the WPTEV was more pronounced. For specimen M68, the WPTEV was 3.3 times that of the healthy specimen, however, the peak-to-peak value was only 2.3 times that of the healthy specimen; (3) The degree of defects was accurately determined by the defect evaluation index (*EI*) based on the WPTEV; (4) The signal was significantly attenuated with the increase in the age of the grouting material, especially in the first three days, and finally the signal achieved a stable value; (5) The numerical simulation indicated that the defects in the length and thickness of the air cavity in the grouting material were efficiently detected by the proposed piezoelectric arrangement in this study.

Keywords: grout sleeve; quality defects; piezoelectric wave method; numerical simulation



Citation: Qiao, Q.; Wang, X.; Liu, W.; Yang, H. Defect Detection in Grouting Sleeve Grouting Material by Piezoelectric Wave Method. *Buildings* **2024**, *14*, 629. <https://doi.org/10.3390/buildings14030629>

Academic Editor: Andreas Lampropoulos

Received: 16 January 2024

Revised: 12 February 2024

Accepted: 22 February 2024

Published: 27 February 2024



Copyright: © 2024 by the authors. Licensee MDPI, Basel, Switzerland. This article is an open access article distributed under the terms and conditions of the Creative Commons Attribution (CC BY) license (<https://creativecommons.org/licenses/by/4.0/>).

1. Introduction

As the most essential part of modern architectural systems, the quality of precast reinforced concrete structures has become a critical issue affecting the safety and durability of the structures. The grouting sleeve connects two precast components, which is the primary connection part of the precast structure. The mechanical properties of the connection mainly depend on the bonding between the grout with steel bars and the inner wall of the sleeve. However, the grouting sleeve connection is concealed in the structure, making it difficult to determine the quality of the connection during inspection. Therefore, it is necessary to apply alternative methods to ascertain the quality and safety performance of the connection [1]. In engineering practice, the quality of grouting is less stringent among construction workers, such as incorrect connection operation of precast components, improper storage of grouting materials, and inadequate anchorage length of steel bars.

Grouting anchoring defects occur due to untimely air removal and insufficient anchoring length, which significantly impact the mechanical properties and serviceability of the grouting sleeve.

Non-destructive testing of grouting sleeves has thus become more and more crucial, and much research has been carried out. Ma et al. [2] evaluated grouting compactness by an acoustic emission system, and showed that the characteristic amplitude and energy distribution were prominent under acoustic emission conditions. Zhang et al. [3] proposed the method of combining acoustic emission and ultrasonic detection to characterize the damage degree of grouting sleeves after tensile loading. Acoustic emission characteristics of grouting sleeves with different damage degrees could be characterized in experiments and simulations. However, expensive equipment and high operational skills were required for acoustic emission. In addition, computed tomography was also used for defect detection in grouting sleeves [4], which required operability accompanied by high radiation. Hence, it is not widely applicable to typical buildings.

The aforementioned detection methods are certainly limited to different construction conditions, making them almost impractical for long-term monitoring. Many drawbacks have been found in the existing non-destructive testing methods, such as the limited detection range of ultrasonic testing methods, which is not suitable for double or multi-row grouting sleeves; acoustic emission has poor sensitivity and expensive equipment is required, limiting the widespread use in practical engineering; and computer tomography has high requirements for operators, strong radiation, and poor safety. In addition, many other non-destructive testing methods, such as electromagnetic testing and vibration testing, have also been used in engineering practice. However, they are limited by materials, the environment, equipment costs, and other factors, affecting their application in the health testing of prefabricated building grouting sleeves. Piezoelectric ceramics are widely used in the field of structural component health testing due to the advantages of small size, high sensitivity, reusability, and low cost. Kaur et al. [5] explored the low-cost electromechanical impedance technique for health monitoring of concrete under destructive testing using multiple piezo configurations. However, the piezoelectric impedance method was highly dependent on the generation of pressure and was not suitable for detecting the degree of initial defects. In addition, the piezoelectric wave method has been widely used in the health monitoring of concrete structures in recent years. Jiang et al. [6] detected the bolt looseness-induced damage in steel truss arch structures. The sensors remained embedded in the concrete to facilitate lifecycle monitoring. Nevertheless, little research on the detection of defects in grouting sleeves has been conducted in precast structures. Detecting the construction quality of grouting sleeves with piezoelectric materials is of great practical significance and an essential step toward the digital transformation of buildings.

Piezoelectric ceramics are small and highly sensitive. Using piezoelectric ceramic-based sensors for structural health monitoring was first proposed by Wang et al. [7], who arranged piezoelectric actuators and sensors as a detecting web in the damaged composite plate to identify structural damage by wave analysis. The received signals were processed by time domain analysis and frequency domain analysis. Zhu et al. [8] monitored the basic mechanical properties and interior damage of concrete structures with a piezoelectric actuator/sensor based on the wave propagation method. Xu et al. [9] detected the debonding at the contact interface of concrete-filled steel tubes using the piezoelectric wave method and investigated the coupling effect of different arrangements of piezoelectric ceramics on the debonding of concrete and steel tubes. It was found that the embedded arrangement approach better reflected the influence of the effect of defect length and depth on the signal. Sun et al. [10] embedded smart piezoelectric modules made of piezoelectric ceramics in concrete to evaluate crack damage. Meng et al. [11] carried out structural health monitoring of reinforced concrete columns under static loading with piezoelectric ceramic drivers and sensors. Yan et al. [12] proposed a health monitoring method for concrete shear walls based on intelligent aggregates, and the damage in different areas was evaluated by an array inside the sensor. Most studies have emphasized defect detection in traditional

components, while few studies have been conducted on quality detection in grouting sleeves, which has limited its implementation at construction sites. Wu et al. [13] tested the grouting compaction in grouting sleeves using piezoelectric ceramics and confirmed the practicality and feasibility of the piezoelectric wave method. Qiao et al. [14] developed semi-grouting sleeves with different defect sizes and identified the defect degree by the stress wave propagation energy in steel bars. Zhu et al. [15] experimentally studied the working conditions of full-scale grouting sleeves with different compaction degrees and proposed a defect evaluation index based on the wavelet packet energy. Du et al. [16] monitored grouting sleeves with different quality defects, including end, middle, and horizontal defects. Cao et al. [17] detected the compactness of the grouting material in sleeves and the wavelet packet energy non-destructive method was first proposed to test the compactness of grouting sleeves.

Considering the feasibility and convenience of piezoelectric ceramics, a convenient and implementable arrangement method of piezoelectric ceramic sheets based on engineering practice has been proposed in this paper. In engineering practice, the same batch of grouting materials and grouting sleeves should be used, and the water–material ratio should also be strictly controlled according to the specifications. The specimens were covered with the same concrete protective layer as at the construction site, and they were cured under constant temperature and humidity conditions in the laboratory for 28 days as healthy specimens. Three to five specimens were required for standard curing, and the average value of the signals was used as the reference signal for healthy specimens. The production method of the standard grouting specimen had the advantages of applicability and simplicity. Aggelis [18] suggested that wave dispersion and frequency-dependent attenuation were more sensitive to damage than the conventional pulse velocity. An easily operated defect detection method in grouting sleeves using piezoelectric ceramics was suggested. Liang et al. [19] indicated that the main factors affecting the bond strength were the compressive strength of the UHPC, the thickness of the cover, and the characteristics of the fiber. A total of 13 semi-grouting sleeves were fabricated with different defects, including holes, air cavities, water-to-binder ratio disparities, and anchoring defects as research variables. Du et al. [20] studied the propagation of stress waves in the pores of cement mortar, which can be used in structural health detection. Signals generated in the experiments were analyzed from the time domain and wavelet packet energy perspective. Three specimens were designed and tested to investigate the effect of the grouting material's age on peak-to-peak values and signal changes were observed at different ages. Gu et al. [21] observed the development of harmonic response amplitude from the embedded piezoelectric sensor at early ages. A finite element model with identical experimental conditions was established in ABAQUS to simulate the piezoelectric wave method under identical experimental conditions, and the effects of air cavity dimensions in grouting sleeves on piezoelectric signals were studied.

2. Piezoelectric Wave Detection Principle and WPTEV

2.1. Piezoelectric Wave Method

A piezoelectric ceramic driver and a piezoelectric ceramic sensor were employed for monitoring in the piezoelectric wave method. An electrical signal was applied to the driver by the signal generator, which was converted into a stress wave signal by the piezoelectric ceramic driver, and the stress wave passed through the sleeve structure. During propagation, the stress wave was reflected or refracted due to the cavities and holes in the grouting material and bonding surface, leading to the signal attenuation of the sensor. The difference between signals received by healthy specimens and specimens with defects was analyzed by processing different signals in the time and frequency domains to detect the defect degree. The detection principle of the piezoelectric wave method is shown in Figure 1.

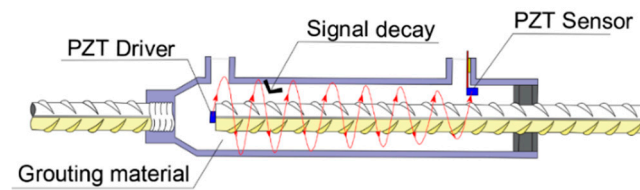


Figure 1. Principle of piezoelectric wave method.

2.2. Basic Theory of WPTEV

Wavelet decomposition is a signal processing method using orthogonal wavelet transform to decompose the low-frequency part of the signal without processing the high-frequency part. The wavelet packet transform is the analysis method that decomposes the high-frequency signal again based on wavelet decomposition. The decomposition process is shown in Figure 2. The method adaptively selects the corresponding frequency band based on the characteristics of the analyzed signals and has few omissions or redundancies, enabling better time–frequency analysis [22].

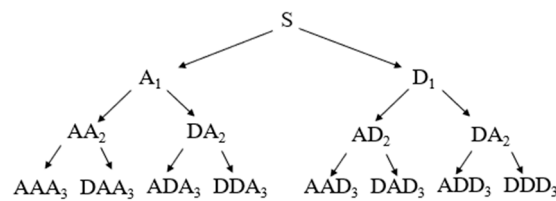


Figure 2. Schematic diagram of wavelet packet decomposition.

Assuming that S is the original monitoring signal, the principle of wavelet packet analysis is to decompose the initial signals into frequency group signals with equal widths, and after N -layer decomposition, the last layer is a 2^N sub-signal with different frequency bands. Then, S can be expressed as shown in Equation (1):

$$S = S_1 + S_2 + \cdots + S_{2^{N-1}} + S_{2^N} \quad (1)$$

In the last layer of the signal, the sub-signal energy vector of each frequency band obtained by wavelet packet decomposition is defined as E_1 , as given in Equation (2) [13]:

$$E_1 = \{e_1, e_2, \cdots, e_{2^{N-1}}, e_{2^N}\} \quad (2)$$

The energy of each frequency band sub-signal in the last layer is given by Equation (3):

$$e_i = \sum_{k=1}^n |x_k|^2 \quad (3)$$

In Equation (3), n is the number of initial sampling points, and x_k is the number of points in each frequency band signal of the last layer after S decomposition and reconstruction.

Then, the wavelet packet energy (E) of signal S is defined as the vector sum of the wavelet packet decomposition and reconstruction signal. E can be expressed by Equation (4):

$$E = \sum_{k=1}^{2^N} e_k \quad (4)$$

3. Experimental Setup

3.1. Experimental Procedure

Three defect-free sleeve specimens and thirteen grouting sleeve specimens with different defects were designed. Piezoelectric ceramic drivers and sensors were embedded within the grouting sleeves to detect the defects. The signal generated by the signal driver

was amplified 100 times by a power amplifier, which acted on the piezoelectric ceramic driver to convert it into the stress wave. The generated stress wave could be received by the piezoelectric ceramic sensor after passing through the grouting material and steel bars, and finally received and displayed by the oscilloscope. The defect degree of the grouting sleeves could be obtained and analyzed by comparing the signal peak value and wavelet packet energy between healthy (without defects) and defective specimens.

A semi-grouting sleeve (type GTJB4-20) was used in this study. The anchorage ends were connected with 20 mm steel bars. A PZT-5A disc-shaped piezoelectric ceramic (5 mm in diameter and 2 mm thick) with a flanging electrode were used. The strength of the grouting material was 60 Mpa. The side where the wires were welded was negative, and its opposite side was used for receiving signals. The specific parameters of the piezoelectric ceramics are presented in Table 1. For the arrangement of the compactness defects in the grouting material, 5 mm diameter foam balls were mixed with the grouting material to simulate the hole defects before grouting the sleeves. Butyl rubber wrapped in the middle of the anchor steel bar was used to simulate air cavity defects of varying thicknesses and lengths.

Table 1. Parameters of piezoelectric ceramic materials.

Material Type	Piezoelectric Constant d_{33} [10^{-12} m/V]	Thickness Frequency Constant [kHz·mm]	Electromechanical Coupling Factor		Mechanical Quality Factor
			k_p [%]	k_t [%]	
PZT-5A	380	2000	0.60	0.45	110

3.2. Experimental Design

The grouting sleeves without defects were used as the standard (control) specimens, and the signals detected by the sensors were used as the reference signal. The extent of the defects in the grouting sleeve was determined by comparison with the standard specimens. Different defects were arranged in the sleeves before grouting, as shown in Figure 3. The arrangement of the specimens is given in Table 2.

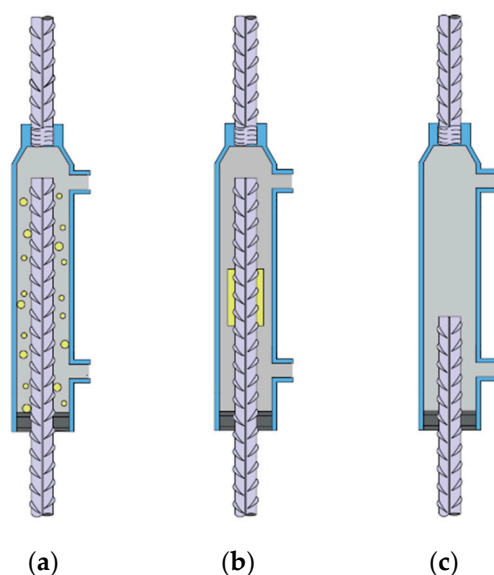
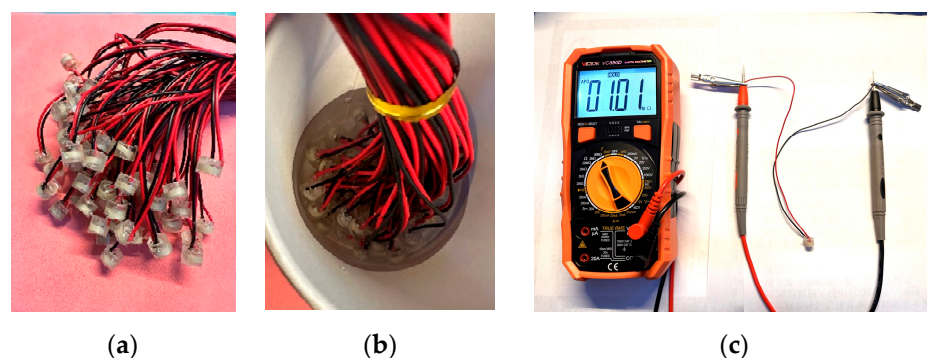


Figure 3. (a) Air hole defects; (b) air cavity defects; (c) defects in anchorage length.

Table 2. Specimen setting and number.

Defect Type	Specimen Number	Degree of Defects
Healthy specimens	H1	--
	H2	--
	H3	--
Compactness defect	D10	Foam pellets account for 10%
	D20	Foam pellets account for 20%
	D30	Foam pellets account for 30%
Grouting air cavity defect (thickness × length)	M34	3 mm × 40 mm air cavity
	M38	3 mm × 80 mm air cavity
	M64	6 mm × 40 mm air cavity
	M68	6 mm × 80 mm air cavity
Water–material ratio defect	S13	The water–material ratio is 0.13.
	S14	The water–material ratio is 0.14.
	S15	The water–material ratio is 0.15.
Reinforcement anchorage defect	A2d	Anchorage length is 2 d
	A4d	Anchorage length is 4 d
	A6d	Anchorage length is 6 d

The arrangement of the piezoelectric ceramics included paste-type drivers and embedded-type sensors. The paste-type sensor was affixed at the center of the smooth section on the top of the anchorage steel bar, whereas the embedded-type sensor was buried 1 mm below the slurry inlet in the sleeve and embedded in the grouting material. In order to prevent damage to the piezoelectric sensors by extrusion or short circuit caused by water contacting the solder joint, the piezoelectric ceramics were placed in the mold, and the waterproof layer of the signal-receiving layer was made of epoxy resin to ensure the stable transmission of stress wave signals at the same time. The thickness of the waterproof layer was about 0.1 mm, and the embedded piezoelectric ceramics were connected with a 1 mm-thick steel wire to fix the piezoelectric ceramics to the slurry inlet. In order to ensure the effectiveness of the waterproof layer, the PZT sheet coated with epoxy resin was placed in water for one hour after the epoxy resin of the waterproof layer was hardened, and a multimeter was used to measure the PZT resistance. The piezoelectric ceramic sheet was equivalent to an open circuit; therefore, the resistance was infinite. The multimeter results indicated good wiring and waterproof conditions [23]. The piezoelectric ceramics are shown in Figure 4.

**Figure 4.** (a) Piezoelectric ceramics; (b) waterproof test; (c) effectiveness test.

A set of piezoelectric ceramics health detection systems was formed after the piezoelectric ceramics were arranged. The grouting sleeves were grouted by the electric grouting

machine, and the grouting was carried out from the slurry inlet. The slurry outlet was blocked with a plug as soon as the grouting material was discharged from the slurry outlet. Meanwhile, the grouting operation was maintained until the mortar volume in the machine was not reduced. The grouting inlet was blocked. After the grouting was complete, the specimens were cured for 28 d in a standard environment. The defect layout and test site are shown in Figure 5.

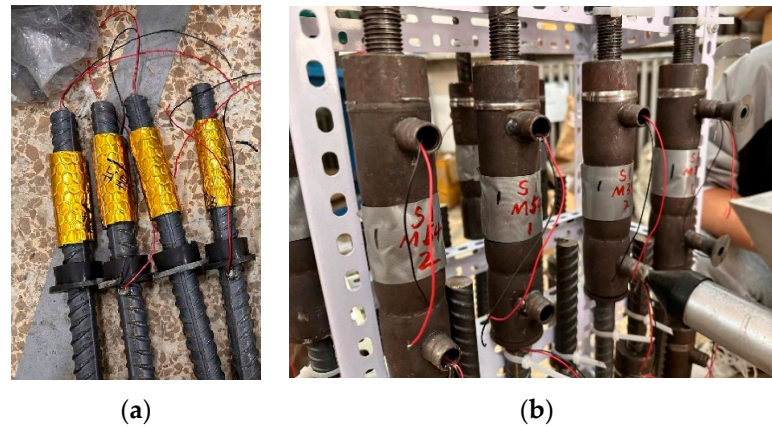


Figure 5. (a) Defect layout; (b) test site.

3.3. Test Equipment

The maximum working frequency of the piezoelectric ceramics was 1 M and the maximum working power was 20 W. The test equipment used in the experiment included the signal generator, high-voltage amplifier, oscilloscope, and personal computer with signal-receiving software. The appropriate signal on the signal generator was selected, which was applied to the piezoelectric ceramic driver after being amplified by the high-voltage amplifier. The stress wave reaching the sensor after propagating through the grouting material, steel bars, and the sleeve was collected by the oscilloscope. The sampling time was 240 μ s. The instruments and connecting devices used in the test are shown in Figure 6.

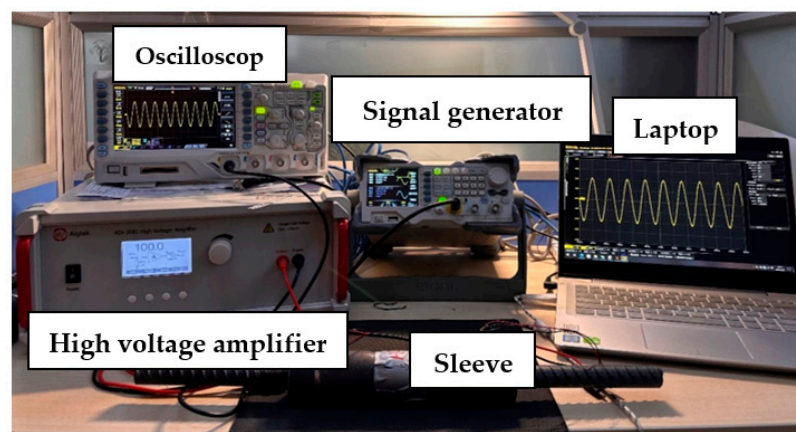


Figure 6. Instruments and equipment used in the test.

3.4. Selection of Signal Frequency

The sinusoidal signal was selected as the driving signal in this study due to the well-shaped waveform and convenience for analysis. In order to select the driving frequency suitable for testing defect detection, a sinusoidal voltage with a peak-to-peak value of 500 V was used. “Peak-to-peak” refers to the potential difference between positive and negative wave peaks. The peak-to-peak values of three defect-free specimens at varying frequencies and the corresponding results are shown in Figure 7. The signal acceptance of

the piezoelectric ceramic sensors was stable within 10–90 kHz. The signal difference was noticeable with increased frequency, and the stability decreased.

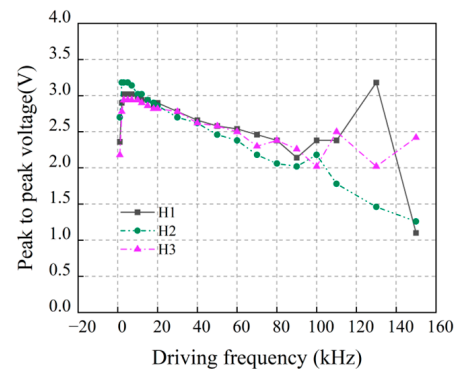


Figure 7. Peak-to-peak values of healthy specimens at different frequencies.

In order to eliminate contingency and ensure the effect of driving frequency on the grouting sleeve specimens with defects, the peak-to-peak values of specimens with different defects at frequencies of 20–130 kHz were further collected. The variation trend in peak-to-peak values was clear under the driving frequencies of 20–80 kHz, as shown in Figure 8. The amplitude attenuation of driving signals less than 100 kHz increased with increasing stress wave frequency. When the frequency exceeded 100 kHz, the signal characteristics of the part of the specimens with defects were unstable, and the stress wave amplitude values fluctuated irregularly. The frequency dispersion effect of the stress wave with the grouting papered in small-volume grouting sleeves changed the wave velocity and propagation path. Thus, 40 kHz was selected as the representative value in this study.

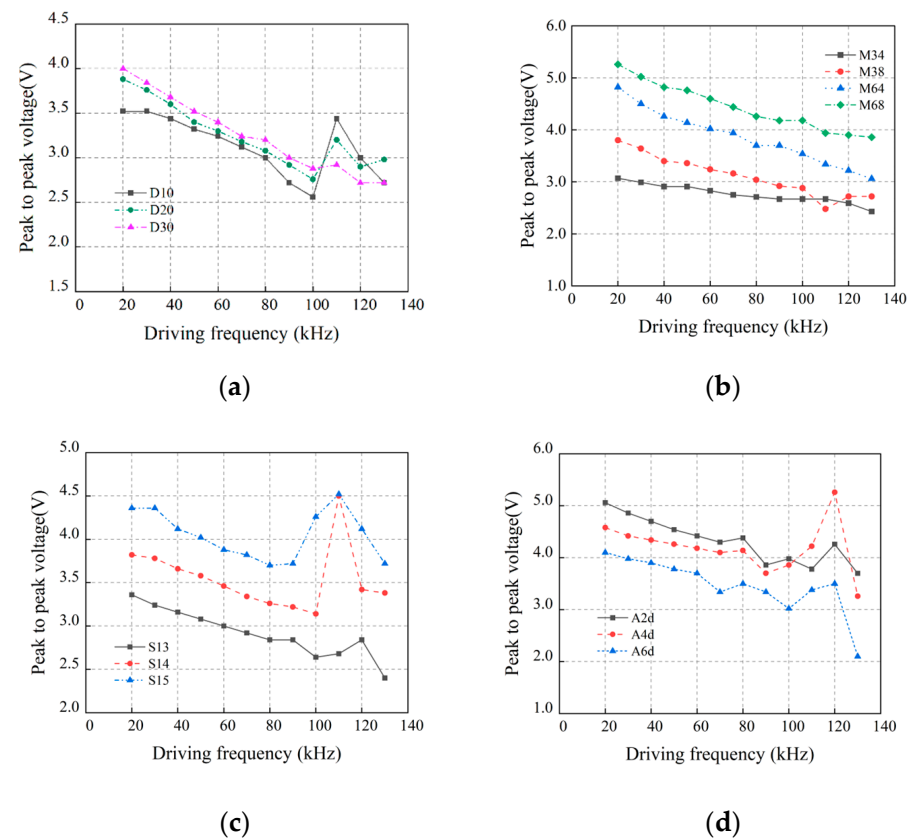


Figure 8. Peak-to-peak values of specimens at different frequencies: (a) compactness defects, (b) air cavity defects, (c) water–material ratio, (d) anchoring defects.

3.5. Signal Analysis of Grouting Material Age

In order to study the effect of the age of the grouting material on the piezoelectric wave signal, three grouting sleeves were designed to test the signal changes in the grouting materials cured to different stages. The test setup was the same as in the previous section, including the signal generator, high-voltage amplifier, oscilloscope, and personal computer. The detection ages of the experiment were set to 3 h, 15 h, 27 h, 39 h, 51 h, 66 h, 78 h, 90 h, 4 d, 5 d, 6 d, 7 d, and 9 d, respectively. Next, 20 kHz, 40 kHz, 60 kHz, and 80 kHz were taken as the driving frequencies and 400 V as the arriving voltage. After the grouting age exceeded 3 days, the peak-to-peak signal values tended to be stable. The experimental results are shown in Figure 9.

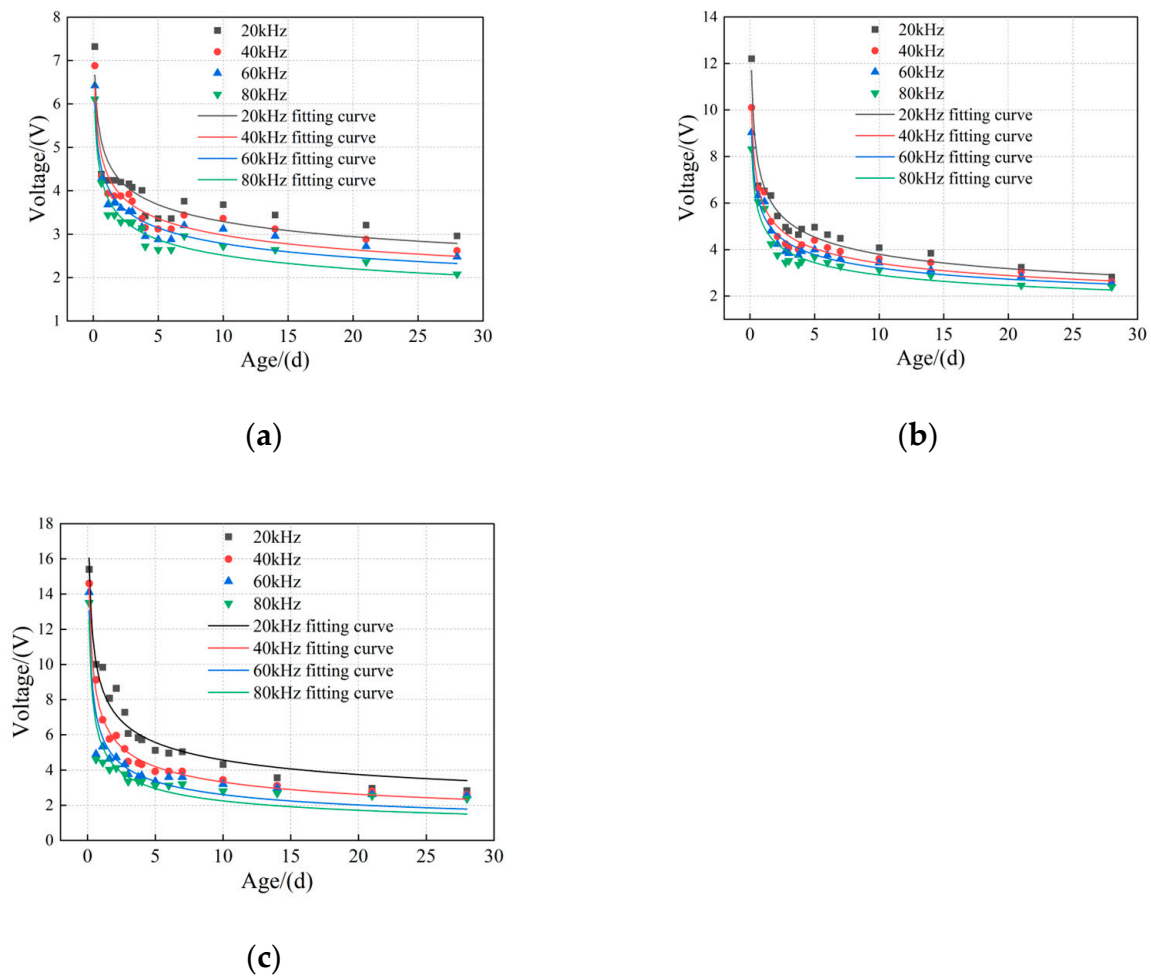


Figure 9. Peak-to-peak values of healthy specimens at different ages: (a) age-1 specimen; (b) age-2 specimen; (c) age-3 specimen.

With the increase in curing age, grout curing resulted in a decreasing trend in signal amplitude. In the whole curing process, the reduction was fast in the early stage, and then became slow. This was due to the fact that the cement hydration was faster in the early stage. In the cement hydration process, the hydration products increased, and the pore structure and pore size distribution of the slurry were constantly changing. When the age increased, the hydration products gradually filled the voids, leading to a denser structure. In the early stage of curing, the hydration reaction was not sufficient, and the stress wave was mainly transferred through the rebar and the sleeve rather than the grouting material. After the early stage of curing, the grouting material gradually reached the maximum degree of

density, and the stress wave was mainly transferred through the grouting material. Thus, the wave attenuation was sharp and the amplitude obviously decreased.

3.6. Signal Characteristics Based on Time Domain Signals

Figure 10 shows the filtered time domain diagram of the signal under various working conditions compared with the reference signal of healthy specimens, in which H3 is the representative value of the reference signal.

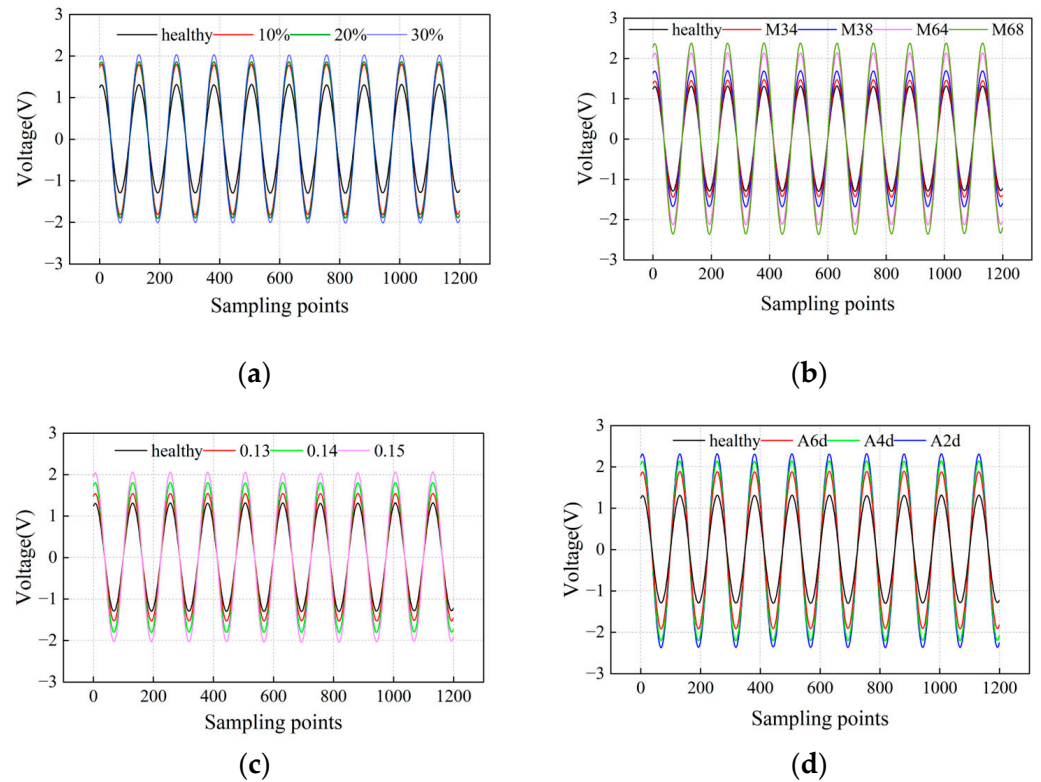


Figure 10. Time domain signals of sensors under different conditions: (a) compactness defects; (b) air cavity defects; (c) water–material ratio defects; (d) anchorage defects.

3.7. Peak-to-Peak Signal Analysis

The time domain signals collected by the sensors under different defects are shown in Figure 10. From the time domain signals, the peak value of each specimen could be read, among which the reference peak value of 2.58 V in the healthy specimen was found to be the smallest. Compared with the peak-to-peak values of the specimens with defects, the voltage increased with the increase in the volume proportion of defects. The peak-to-peak value for each specimen is listed in Table 3 and shown in Figure 11.

Table 3. Peak-to-peak voltage of each specimen.

Defect Type	Healthy Specimen	Compactness Defect			Air Cavity Defect				Water–Material Ratio Defect			Reinforcement Anchorage Defect		
		10%	20%	30%	M34	M38	M64	M68	0.13	0.14	0.15	A6d	A4d	A2d
Specimen number	H3	10%	20%	30%	M34	M38	M64	M68	0.13	0.14	0.15	A6d	A4d	A2d
Peak-to-peak value	2.58	3.57	3.75	4.02	2.88	3.34	4.34	4.72	3.08	3.61	4.06	3.74	4.27	4.62

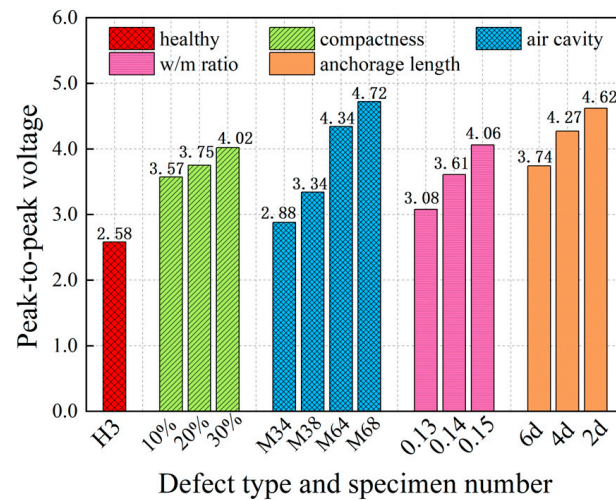


Figure 11. Peak-to-peak voltage of each specimen.

Compared with the reference specimen, the air cavities or holes in the grouting material had almost zero transmission ability for stress waves. Similarly, the increasing water-to-binder ratio led to increased free water in the grout, which expanded the volume of holes and hindered stress wave propagation. The volume of the grouting material decreased with the increase in the air volume ratio or the ratio of water, facilitating more stress waves passing through the steel and less through the grouting material. Hence, as the low-amplitude stress wave received by the piezoelectric ceramic sensor decreased, the total amplitude of the stress wave received by the piezoelectric ceramics increased. As the converted voltage signal increased with the increase in defect rate, the received signal showed a gradual increase in peak value.

3.8. Wavelet Packet Energy Analysis Method

The size of the wavelet packet energy value can also be used to ascertain the damage degree. In this study, the driving signal was a unique frequency, and the energy after wavelet packet decomposition was mainly concentrated in the low-frequency part. Considering the air cavity defects as an example, wavelet packet decomposition could be used to obtain the energy values of each decomposition group in the last layer of decomposition, as presented in Table 4. The results indicated that the energy of the first frequency band in the last layer accounted for about 99.7% of the total energy, whereas the signals in the other frequency bands were not obvious. Therefore, the WPTEV was selected instead of the energy values of each frequency band for a more intuitive signal analysis. In this paper, “sym4” was selected as the wavelet basis, and the measured signal was decomposed into three layers; then, the signal was reconstructed to obtain the WPTEV for this specimen. The result of the WPTEV of the last layer of the received signal is shown in Figure 12.

Table 4. Decomposition energy of each frequency band in the last layer of the air cavity defect specimen.

Specimen Number	WPTEV	0th	1st	2nd	3rd	4th	5th	6th	7th
Healthy	1100.29	1096.67	0.06	0.07	0.17	0.07	0.10	0.14	3.01
M34	1365.59	1361.76	0.08	0.09	0.18	0.08	0.11	0.12	3.19
M38	1856.39	1852.10	0.08	0.05	0.08	0.05	0.06	0.10	3.88
M64	2952.69	2947.35	0.10	0.05	0.06	0.06	0.05	0.12	4.90
M68	3630.75	3617.14	0.28	0.32	0.44	0.26	0.34	0.41	11.57

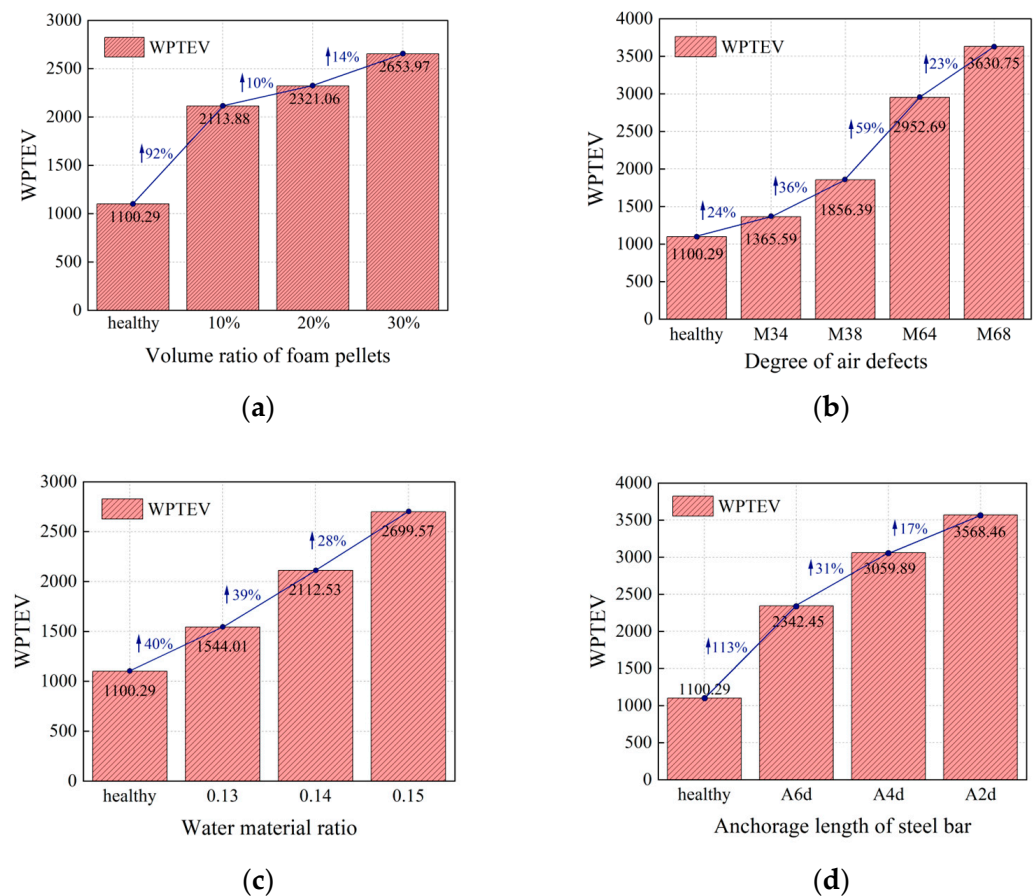


Figure 12. Wavelet packet total energies of different defect specimens: (a) compactness; (b) air cavity defect; (c) water–material ratio defect; (d) anchorage length defect.

Consistent with the results of the peak-to-peak values, the wavelet packet energy was the smallest for the healthy specimen without defects, as shown in Figure 12. The rising arrow in the Figure 12 indicates the specific numerical variation of WPTEV with the increase of defect severity. The wavelet packet energy gradually increased with the volume proportion of air cavity defects. When the defect degree reached M68, the wavelet packet energy increased to 3.3 times that of the non-defect specimen. As the volume ratio of foam balls in the grout increased, the wavelet packet energy gradually increased. The wavelet packet energy could more directly show the impact of cavity defects on the signal value. When the volume ratio of foam balls was 10%, the wavelet packet energy increased to 1.9 times. As the anchorage length changed, the change in wavelet packet energy value increased with the decrease in anchorage length. When the anchorage length was only 2 d (d is the bar diameter), the signal growth was 3.24 times that of the healthy specimen. The increase in the water-to-binder ratio also increased the wavelet packet energy. When the water-to-binder ratio was 0.15, the wavelet packet energy became 2.45 times that of the healthy specimen. With the change in defect degree, the variation trend in the wavelet packet energy value was consistent with the change in output voltage amplitude measured directly by the experiment. Hence, the change in wavelet packet energy value was more intuitive.

3.9. Damage Evaluation Indicators

Figure 12b shows that the change in wavelet packet energy value caused by the variation in thickness direction was more significant than the change caused by the variation in length direction. The sensor could not receive the signal when the grouting material was empty. The research focus of this study was air defects in fully grouted specimens; thus,

the detection signal of the entire defect could not be received in the experiment. In order to ascertain defect evaluation indicators, and considering the on-site situation of precast part connections, the defect level of M68 had almost reached the maximum defect level of grouting, and any larger defect level was not considered.

While establishing defect evaluation indicators, the WPTEV should be used as the theoretical energy value of full defects. Therefore, the evaluation indicator (*EI*) for grouting sleeves can be defined as shown in Equation (5):

$$EI_a = \frac{E_a - E_h}{E_M - E_h} \quad (5)$$

where E_a and E_h represent the WPTEV of a test specimen and healthy specimen, respectively; and E_M denotes the energy value of the wavelet packet for the M68 specimen. The damage evaluation indicators of each specimen were calculated using Equation (5), and the calculation results are presented in Table 5 and Figure 13. Table 5 indicates that the *EI* of M68 was 1.0. Compared to this, the *EI* of each kind of specimen increased with the increase in defect degree. This indicator proved that the evaluation index proposed based on the WPTEV could effectively reflect the degree of internal defects in the grouting sleeve.

Table 5. *EI* of each specimen.

Defect Type	Healthy Specimen	Compactness Defect			Air Cavity Defect				Water–Material Ratio Defect			Reinforcement Anchorage Defect		
		10%	20%	30%	M34	M38	M64	M68	0.13	0.14	0.15	A6d	A4d	A2d
Specimen number	H3	10%	20%	30%	M34	M38	M64	M68	0.13	0.14	0.15	A6d	A4d	A2d
<i>EI</i>	0	0.40	0.48	0.62	0.10	0.30	0.74	1.0	0.18	0.40	0.64	0.50	0.78	0.98

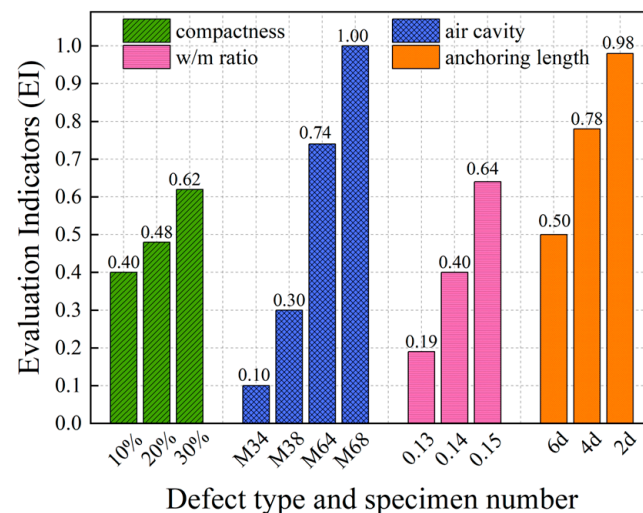


Figure 13. *EI* of each specimen.

In summary, the extent of grouting sleeve defects could be determined based on the *EI* values proposed by the WPTEV. Based on this study, when the *EI* value is less than 0.6, the degree of defect in the sleeve is relatively mild; when the *EI* value is between 0.6 to 1.0, the degree of defects inside the sleeve is relatively severe, affecting its mechanical performance; and in practical engineering, if the *EI* value is greater than 1.0, the degree of defects is severe, and the sleeve has almost no tensile capacity.

4. Numerical Simulations

4.1. Defining Material Properties

Ignoring the influence of the inner ribs of the sleeve on signal propagation, the ABAQUS model employed the same size and piezoelectric ceramic arrangement method as was used in the experiments. Since the testing procedure was non-destructive, it was completed in the material elastic stage, and only its elastic properties were defined when defining the material. The densities of the sleeve and steel bar were 7850 kg/m^3 and 7800 kg/m^3 , respectively, while the elastic modulus and Poisson's ratio of both were taken as $2.06 \times 10^5 \text{ MPa}$ and 0.3 , respectively. The density of the grouting material was 2300 kg/m^3 , while the elastic modulus and Poisson's ratio were $3.5 \times 10^5 \text{ MPa}$ and 0.2 , respectively.

Due to the intrinsic defects in the grouting material, the original stress wave was attenuated when the stress wave encountered reflection and refraction at different interfaces. To simplify the model, the grouting material was assumed to be a uniform elastic medium with Rayleigh damping, including mass damping and stiffness damping, to compensate for the influence of the microstructure on the numerical simulation. Rayleigh damping is a linear combination of mass and stiffness matrices, as given in Equation (6):

$$[C] = \alpha[M] + \beta[K] \quad (6)$$

where α and β are the damping coefficients of mass and stiffness, respectively. α mainly suppresses the low-frequency part, while β mainly suppresses the high-frequency part. As the frequency of the driving signal used in the study was in the high-frequency range, α could be ignored. Thus, damping mainly depended on the β value in this study [24].

The piezoelectric ceramic plates used in this simulation were both E-type boundary conditions. The E-type constitutive equation of piezoelectric ceramics is given by Equation (7) [25]:

$$\begin{aligned} T &= c^E S - e^T E \\ D &= e S + \epsilon^S E \end{aligned} \quad (7)$$

where D and E denote the electric displacement vector and the electric field intensity vector, respectively; S and T indicate the strain vector and the stress vector, respectively; c^E and ϵ^S are elastic stiffness matrix and dielectric constant matrix, respectively; e is the piezoelectric stress constant matrix; and e^T is the transpose matrix for e .

4.2. Contact and Load Setting

The contacts in this simulation were all tie contacts, comprising contact pairs of the grouting sleeve and grouting material, reinforcement and grouting material, reinforcement and piezoelectric ceramic driver, and concrete and piezoelectric ceramic sensor.

Before loading, the upper surface of the sleeve was completely fixed, limiting the translational and rotational degree of freedom in the X, Y, and Z directions. Before loading the excitation signal, the contact surface between the piezoelectric ceramic driver and the steel bar was regarded as the grounding end. The other electrode surface was regarded as the driving voltage input end. The grounding end was defined as zero potential. The arrangement of the sensors was the same as for the driver.

In order to reduce the dispersion effect and supplement the experimental conditions [26], the Hanning modulation window function with $f = 40 \text{ kHz}$ modulated the central frequency and $V_0 = 10 \text{ V}$ amplitude was input at the driving end of the piezoelectric ceramics. The time history curve of the excitation signal is shown in Figure 14.

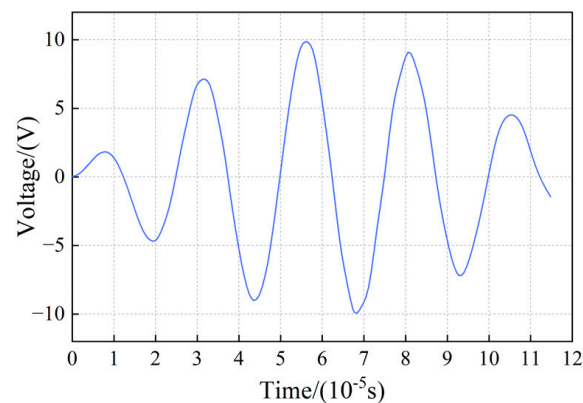


Figure 14. Time history diagram of the excitation signal.

4.3. Grid Division and Analysis Steps

The grid size (l) in this simulation was $1/10$ of Rayleigh wavelength λ , as shown in Equation (8). Due to the small size of the piezoelectric ceramics, the grid of piezoelectric ceramics and the horizontal space of concrete where the sensor was embedded were selected for local refinement. In this model, the structured grid division method was used. The C3D8E piezoelectric grid element was chosen for the piezoelectric ceramics, while the C3D8R stress grid element was selected for the grouting material, grouting sleeve, and reinforcement. The model after grid division is shown in Figure 15. The grouting sleeve is represented in red, the grout material is represented in green, and the steel reinforcement is represented in white.

$$l < \frac{\lambda}{10} \quad (8)$$

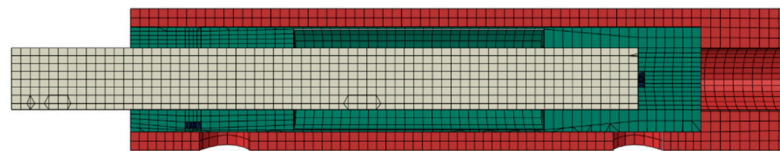


Figure 15. Grid division section of the grouting sleeve.

The higher the driving signal frequency, the smaller the integration time step [27]. When Equation (9) is satisfied, the finite element model can ensure convergence and accurately capture stress waves.

$$\Delta t < \frac{l}{20f} \quad (9)$$

where Δt is the integration time step and f is the excitation signal frequency. In this paper, the frequency of the excitation signal was 40 kHz. It was finally determined that the grid size of the concrete and grouting material was 3 mm. The time increment step was set to $\Delta t = 1 \times 10^{-9}$. The total analysis step time is 0.03 s.

4.4. Stress Diagram of the Propagation Path of the Grouting Sleeve with Air Cavity Defect

The stress diagram of the grouting sleeve with air cavity defects at different times is shown in Figure 16. The air cavity defects affected the stress wave propagation path. Under different air cavity defects, the stress wave was first emitted by the PZT driver, then propagated through the steel bars, sleeves, and grouting material, finally reaching the PZT sensor. In the healthy specimen, the grouting material volume was the largest and the stress noticeably decreased when it passed through the grouting material, so the energy dissipation was the largest. In contrast, in the specimen with air cavity defects, the stress wave propagation in the air cavity was blocked. The proportion of the stress wave propagating through the grouting material to the sensor decreased, along with the

scattering and refraction energy and attenuation of the stress wave in the propagation process, and the voltage was improved.

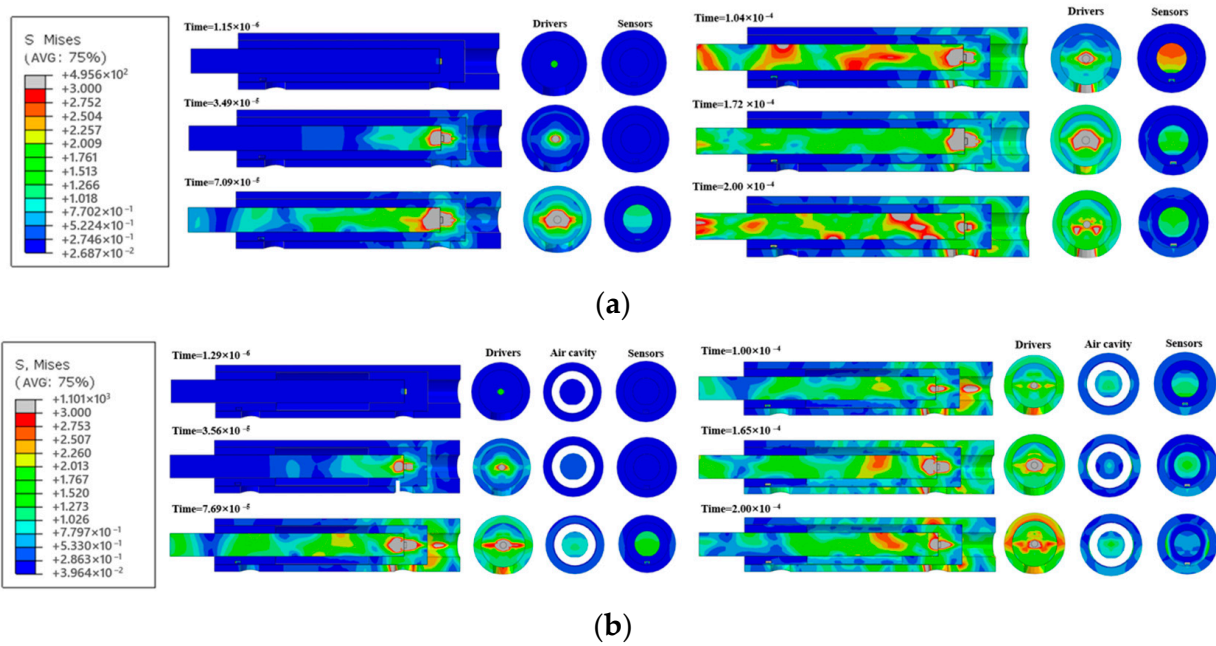


Figure 16. Stress diagram of specimens with defects and healthy specimens without defects: (a) non-defective specimens; (b) specimens with defects.

4.5. Finite Element Simulation and Analysis of Air Cavity Defects in Grouting Sleeves

An air cavity defect in the middle of the grouting sleeve was established, consistent with the test conditions. Air chambers with lengths of 40 mm and 80 mm were set for thickness dimensions of 3 mm and 6 mm, respectively. The influence of different defects on the output voltage is shown in Figure 17.

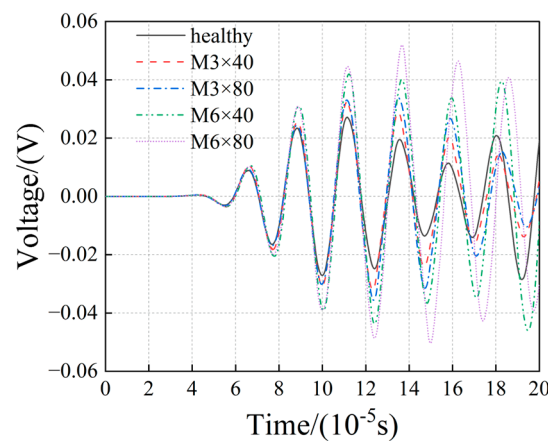


Figure 17. Different air cavity defect sensor signals.

Figure 17 shows that the air cavity reduced the grouting material volume through which the stress waves passed. Consequently, the attenuated signal decreased, and the signal amplitude output by the healthy specimen with the largest grouting volume was the smallest. The signal amplitude gradually increased with the increase in the air cavity depth. In contrast, with the increase in the air cavity defect thickness, the signal amplitude presented the same pattern of change. Due to experimental limitations, the simulation and analysis were conducted in ABAQUS to explore the influence of length and thickness on the signal.

4.6. Finite Element Detection Results of Air Cavity Defects in Length and Thickness

The 6 mm-wide air cavity defect lengths were set to 20 mm, 40 mm, 60 mm, and 80 mm, respectively, in the grouting sleeve, and eventually, the signal change caused by structural damage was analyzed. The output signal voltage amplitudes of the grouting sleeves with different length defects are shown in Figure 18. Likewise, the 40 mm-long air cavity defect widths were set to 2 mm, 4 mm, and 6 mm, respectively. The output signals of the grouting sleeve with different thickness defects are shown in Figure 19, while the results of the wavelet packet energy analysis using Python are shown in Figures 20 and 21. The rising arrow indicates the specific numerical variation of WPTEV with the increase of defect severity.

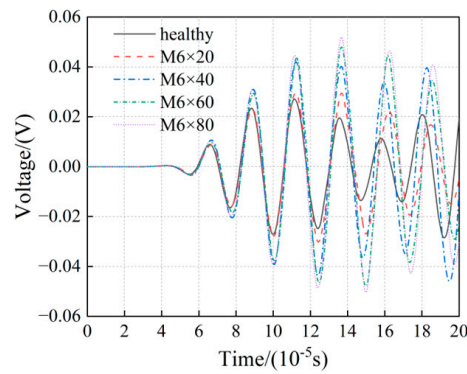


Figure 18. Signals of air cavity defect sensors with different lengths.

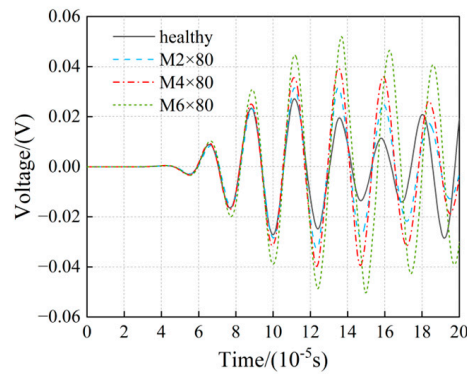


Figure 19. Signals of air cavity defect sensors with different thicknesses.

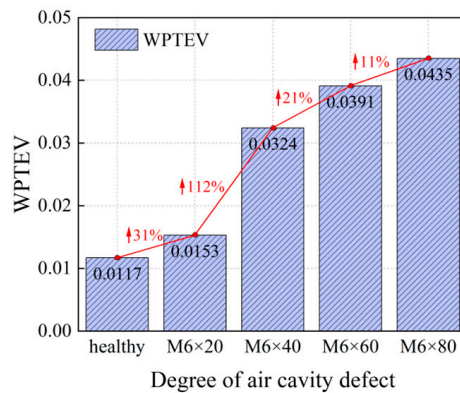


Figure 20. Wavelet packet energy of air cavity defects with different lengths.

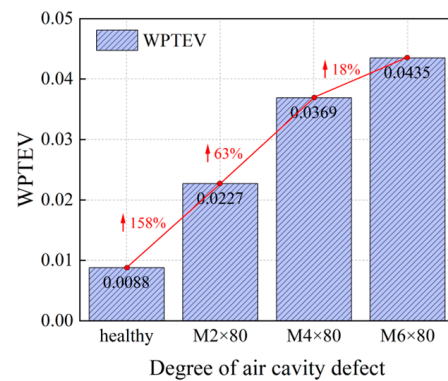


Figure 21. Wavelet packet energy of air cavity defects with different thicknesses.

Figures 18–21 indicate that air cavity defects reduced the grouting volume, and the weakening effect on the stress waves was reduced. Thus, the amplitude of signals received by the sensor increased. With the increasing length of air cavity defects, the amplitude of the sensor output signals increased. In summary, the wavelet packet energy value increased more obviously. Further, with the increase in the air cavity defect thickness, the amplitude of the sensor signal value increased and the wavelet packet energy value increased. Therefore, the accuracy of the simulated results in this paper was well corroborated.

5. Conclusions

A piezoelectric ceramic scheme was proposed for defect detection in grouting sleeves in this paper, which was suitable for precast structures. The drivers and sensors were arranged in the sleeve, and the piezoelectric wave method was utilized. The grouting sleeve specimens with different defects were tested and simulated, validating the feasibility and accuracy of the detection scheme proposed in this study. The following conclusions were drawn from the obtained results.

1. Piezoelectric ceramics can effectively identify the defects in grouting sleeves with different degrees. The peak value of the signal can help preliminarily determine whether the defects are involved in the grouting sleeve.
2. As the curing age of the grouting material increases, the peak-to-peak voltage of the grouting sleeve decreases sharply in the first three days, then slows in the later stage.
3. The air cavity defects and the increase in the volume ratio hinder stress wave propagation. The increase in compactness defects also restricts signal propagation. The voltage output amplitude gradually increases with the increase in volume ratio of defects in the grouting material. Among them, when the cavity volume only accounted for 10%, the amplitude increased to 1.9 times that of the healthy specimen.
4. The analyzed WPTEV of the sensor gradually increases with the increase in air cavity and compactness defects. The results of the wavelet packet energy value are more intuitive. For example, when the air cavity defect was M68 in the test, the wavelet packet energy value was 3.3 times that of the healthy specimen, but the peak-to-peak value was only 2.3 times that of the healthy specimen. The peak-to-peak value and the wavelet packet energy value can provide a basis for defect detection in grouting sleeves.
5. The signal amplitude of healthy specimens was found to be the lowest according to the results of finite element simulation. The signal amplitude of the piezoelectric ceramic sensors increases with the length or thickness of air cavity defects.
6. The evaluation index (*EI*) calculated based on the WPTEV has a relatively accurate defect identification ability.

Author Contributions: Methodology, Q.Q.; Software, X.W.; Formal analysis, X.W.; Investigation, W.L. and H.Y.; Resources, Q.Q., W.L. and H.Y.; Writing—original draft, X.W.; Writing—review & editing, Q.Q.; Project administration, W.L. All authors have read and agreed to the published version of the manuscript.

Funding: This research was funded by the Ministry of Science and Technology of the People's Republic of China grant number (2019YFD1101003).

Data Availability Statement: The data presented in this study are available on request from the corresponding author. The data are not publicly available due to confidentiality agreement signed with the data provider.

Conflicts of Interest: Authors Wenchao Liu and Hongchun Yang were employed by the company CCCC Construction Group Co., Ltd. The remaining authors declare that the research was conducted in the absence of any commercial or financial relationships that could be construed as a potential conflict of interest.

References

- Zheng, Q. Experimental Study on Effects of Grouted Defects on Behaviors of Grout Sleeve Splicing and Specimens. Master's Thesis, China Academy of Building Research, Beijing, China, 2017. Available online: https://kns.cnki.net/kcms2/article/abstract?v=yXT3uqWUX_0J6U_S1eFkpRPAPj47-gKVvHutiJhudmkj0-x6tUkeYC9xdc823y4-xgThhoLA8uOpPOzLumOgJHN1E08Cy7DIW4E_7RUYgq97RHELKn1I7dfCFbz3eo_z-a1QTxjI=&uniplatform=NZKPT&language=CHS (accessed on 15 January 2024).
- Ma, Y.F.; Li, S.L.; Wu, Y.Q.; Wang, D.W.; Liu, M.Y. Acoustic emission testing method for the sleeve grouting compactness of fabricated structure. *Constr. Build. Mater.* **2019**, *221*, 800–810. (In Chinese) [[CrossRef](#)]
- Zhang, L.; Fang, Z.M.; Tang, Y.Z.; Li, H.Y.; Liu, Q.Z. Characterization of Damage Progress in the Defective Grouted Sleeve Connection Using Combined Acoustic Emission and Ultrasonics. *Sensors* **2022**, *22*, 8579. [[CrossRef](#)] [[PubMed](#)]
- Guo, T.; Yang, J.; Wang, W.; Li, C. Experimental investigation on connection performance of fully-grouted sleeve connectors with various grouting defects. *Constr. Build. Mater.* **2022**, *327*, 126981. [[CrossRef](#)]
- Kaur, N.; Li, L.F.; Bhalla, S.; Xia, Y. A low-cost version of electro-mechanical impedance technique for damage detection in reinforced concrete structures using multiple piezo configurations. *Adv. Struct. Eng.* **2017**, *20*, 1247–1254. [[CrossRef](#)]
- Jiang, T.Y.; Wu, Q.L.; Wang, L.; Huo, L.S.; Song, G.B. Monitoring of Bolt Looseness-Induced Damage in Steel Truss Arch Structure Using Piezoceramic Transducers. *IEEE Sens. J.* **2018**, *18*, 6677–6685. [[CrossRef](#)]
- Wang, C.S.; Chang, F.K. Built-in diagnostics for impact damage identification of composite structures. In Proceedings of the 2nd International Workshop on Structural Health Monitoring, Stanford, CA, USA, 8–10 September 1999; pp. 612–621.
- Zhu, J.S.; He, L.K. Piezoelectric Actuator/Sensor Wave Propagation Based Nondestructive Active Monitoring Method of Concrete Structures. *J. Wuhan Univ. Technol. Mater. Sci. Ed.* **2011**, *26*, 541–547. [[CrossRef](#)]
- Xu, B.; Chen, H.B.; Mo, Y.L.; Chen, X.M. Multi-physical field guided wave simulation for circular concrete-filled steel tubes coupled with piezoelectric patches considering debonding defects. *Int. J. Solids Struct.* **2017**, *122*, 25–32. [[CrossRef](#)]
- Sun, W.; Du, J.; Qiao, P.; Qi, B.; Yan, S.; Tan, H. Smart piezoelectric module-based wave energy measurement for crack damage evaluation of concrete beams. *Measurement* **2023**, *221*, 113463. [[CrossRef](#)]
- Meng, Y.Y.; Yan, S.; Sun, W. Experimental research on damage detection of concrete structures based on piezoelectric smart aggregates. In Proceedings of the 2nd International Conference on Civil Engineering, Architecture and Building Materials (CEABM 2012), Yantai, China, 25–27 May 2012; pp. 1145–1151.
- Yan, S.; Sun, W.; Song, G.B.; Gu, H.C.; Huo, L.S.; Liu, B.; Zhang, Y.G. Health monitoring of reinforced concrete shear walls using smart aggregates. *Smart Mater. Struct.* **2009**, *18*, 047001. [[CrossRef](#)]
- Wu, C.; Yang, C.; Ma, S.L.; Xu, X.L. Feasibility Study on Grouting Compactness Detection in Sleeves Using Piezoelectric Transducers. *Appl. Sci.* **2020**, *10*, 149. [[CrossRef](#)]
- Longxi, Q.; Yang, X.; Xiaosheng, L.; Guowen, Z.; Yunpeng, X.; Bin, X.; Song, X. Experiment on Defect Detection for Grouting Splice Sleeves Based on Piezoelectric Wave Measurement Method. *Piezoelectr. Acousto-optics* **2022**, *44*, 955–960. (In Chinese)
- Zhu, H.; Sun, Y.; Dong, Z.; Chen, D.; Wu, G. Reserch on defect and Stress Propagation Simulation of Grouting Sleeve Based on Piezoelectric Ceremics. *J. Archit. Civ. Eng.* **2022**, *39*, 117–126. (In Chinese)
- Yongfeng, D.; Jinfu, D. Research on recognition of sleeve grouting quality defects based on piezoelectric wave method. *Build. Struct.* **2021**, *51*, 49–55. (In Chinese)
- Cao, D.; Pan, Z.F.; Zhang, Z.; Zeng, B. Study on non-destructive testing method of grouting sleeve compactness with wavelet packet energy ratio change. *Constr. Build. Mater.* **2023**, *389*, 131767. [[CrossRef](#)]
- Aggelis, D.G. Damage Characterisation of Inhomogeneous Materials: Experiments and Numerical Simulations of Wave Propagation. *Strain* **2011**, *47*, 525–533. [[CrossRef](#)]
- Liang, R.; Huang, Y.; Xu, Z.M. Experimental and Analytical Investigation of Bond Behavior of Deformed Steel Bar and Ultra-High Performance Concrete. *Buildings* **2022**, *12*, 460. [[CrossRef](#)]

20. Yu, Z.; Ping, C.; Bin, X.; Qing, H. Experimental Study on Interface Debonding Detection of Concrete-filled Steel Tubular with Embedded PZT. *Constr. Technol.* **2014**, *43*, 384–388. (In Chinese)
21. Du, C.C.; Zou, D.J.; Liu, T.J.; Lv, H.X. An exploratory experimental and 3D numerical investigation on the effect of porosity on wave propagation in cement paste. *Measurement* **2018**, *122*, 611–619. [[CrossRef](#)]
22. Gu, H.; Song, G.; Dhonde, H.; Mo, Y.L.; Yan, S. Concrete early-age strength monitoring using embedded piezoelectric transducers. *Smart Mater. Struct.* **2006**, *15*, 1837–1845. [[CrossRef](#)]
23. Yu, Z. *Research on Influencing Factors of Performance of Piezoelectric Smart Aggregate*; Shenyang Jianzhu University: Shenyang, China, 2018. (In Chinese)
24. Song, F.; Huang, G.L.; Kim, J.H.; Haran, S. On the study of surface wave propagation in concrete structures using a piezoelectric actuator/sensor system. *Smart Mater. Struct.* **2008**, *17*, 055024. [[CrossRef](#)]
25. Xinling, F.; Bin, X.; Song, X. Number Simulation Study on Stress Wave Propagation in Grouting Sleeve With Defects. *Piezoelectrics Acoustooptics* **2019**, *41*, 793–796. (In Chinese)
26. Guoli, S.; Jingliang, L.; Xianying, Y.; Jinfu, W.; Wenting, Z. Defect detection of sleeve grouting based on stress wave of piezoelectric ceramics. *J. Fujian Univ. Technol.* **2019**, *17*, 586–592. (In Chinese)
27. Moser, F.; Jacobs, L.J.; Qu, J.M. Modeling elastic wave propagation in waveguides with the finite element method. *NDT E Int.* **1999**, *32*, 225–234. [[CrossRef](#)]

Disclaimer/Publisher’s Note: The statements, opinions and data contained in all publications are solely those of the individual author(s) and contributor(s) and not of MDPI and/or the editor(s). MDPI and/or the editor(s) disclaim responsibility for any injury to people or property resulting from any ideas, methods, instructions or products referred to in the content.